Journal of African Earth Sciences 57 (2010) 444–454

Contents lists available at ScienceDirect

Journal of African Earth Sciences

journal homepage: www.elsevier.com/locate/jafrearsci

Sequential extraction of labile elements and chemical characterization of a basaltic soil from Mt. Meru, Tanzania

M.G. Little [a,*], C.-T.A. Lee [b]

[a] Biology Department, Duke University, Box 90338 Durham, NC 27708, United States
[b] Department of Earth Sciences, Rice University, MS-126, 6100 Main Street, Houston, TX 77005, United States

ARTICLE INFO

Article history:
Received 6 April 2009
Received in revised form 23 November 2009
Accepted 1 December 2009
Available online 5 December 2009

Keywords:
Soil formation
Sequential extraction
Chemical weathering
Tanzania

ABSTRACT

We conducted a modified Bureau Commun Reference (BCR) sequential extraction on a basaltic soil (phono-tephrite) from Mt. Meru in Northern Tanzania in order to determine the relative contribution of water soluble, carbonate and exchangeable, oxide and organic fractions to the bulk composition of the soil. Elemental compositions were determined by ICP-MS and corrected for loss on ignition. Relatively immobile elements, such as Zr, Hf and Al, are enriched by 10–30% compared to the unweathered protolith, consistent with soil formation being accompanied by mass loss due to chemical weathering. However, superimposed on this mass loss appears to be enrichment of elements such as Fe, Ca and Mg, especially towards the surface. In some cases, the bulk concentrations of these elements at the surface exceed that of the protolith. These data suggest that the surface of the Meru soil columns may have experienced "re-fertilization" by the deposition of volcanic ash. From the carbonate and exchangeable extraction, we found evidence of clay rich horizons which may sequester as much as 5% of the bulk K. The concentration of calcium carbonate appears to decrease with depth, but the largest incorporation of Sr and Ba into carbonates occurs below 114 cm. Fe and Mn oxides scavenge more than 10–20% of total Ti, V, Co, Cu, Zr and Pb below 114 cm. The organic fraction sequestered significant fractions of total Al, Cu, REE's and Pb throughout the soil column.

1. Introduction

Natural soil quality is important for small holder faming, the dominant form of agriculture in East Africa (Rockström and Killingtveit, 2003; Stocking, 2003). Most small holder farmers have limited access to fertilizers; therefore, primary soil quality, conservative farming practices and, when available, manure or other organic materials are the basis for soil productivity (Kaizzi et al., 2007). The East African Plateau, including most of Tanzania, is subject to gully erosion (observed firsthand by the authors) which is exacerbated by overgrazing and changing climate trends (Mati 2005; Boko et al., 2007; Vaje et al., 2005). In Tanzania, rapidly increasing rural population and the growth of a market economy for agricultural products has also increased demands on soil fertility across the country (Potts, 2009; Mati, 2005). Understanding the geochemical composition of the soils that are new to cultivation, such as the forested mountain slopes in northern tanzania, is key to understanding their vulnerability to overuse and their resistance to leaching.

The northern provinces of Tanzania lie in the East African rift valley, a large, complex faulting domain in Ethiopia, Kenya and Tanzania. Relatively recent tectonic activity in Northern Tanzania (<2.5 mya) has created a low lying region which is home to lakes (e.g., Lakes Natron and Amboseli) and numerous volcanoes (Dawson, 1992; MacIntyre et al., 1974). Mt. Meru is a large, pyroclastic volcano in this region with a history of activity that dates from about 2 mya into the Holocene (Wilkinson et al., 1986). Present-day Mt. Kilimanjaro, like Mt. Meru to the wast, is marked by a wet climate on the southern flank (Røhr and Killingtveit, 2003). The objective of this study was to assess the mobility of major, minor and trace elements during chemical weathering of a basaltic protolith through a case study of a basaltic (phono-tephrite) soil profile on the southern slopes of Mt. Meru. Much work has been done investigating various pedologic characteristics of tropical volcanic soils from element mobility (Kurtz et al., 2000) to the fate of heavy metals (Palumbo et al., 2000). Of particular interest are the extent of element mobilization in the bulk soil and the absorption of elements by authigenic phases. In order to analyze the authigenic phases, we performed a series of chemical extractions intended to separate the water soluble, carbonate and exchangeable, oxide and organic soil fractions. Our bulk chemistry data allow us to quantify net chemical losses from the soil during weathering as well as net mass additions by other processes such as atmospheric dust deposition. The extractions elucidate phase distribution within the soil column during soil formation and

* Corresponding author. Tel.: +1 919 616 8214.
E-mail address: mglittle@alumni.rice.edu (M.G. Little).

1464-343X/$ - see front matter © 2009 Elsevier Ltd. All rights reserved.
doi:10.1016/j.jafrearsci.2009.12.001

may aid future assessments of viability for continued agricultural exploitation. Our analyses also provide insight into the fate and transport of heavy metals which may become important for public environmental health if anthropogenic sources for these metals increase.

2. Materials and methods

2.1. Sample description

Samples were collected from soils formed on a massive basalt flow northern Tanzania on the southern slope of the main cone of Mt. Meru (03°19.604′S, 36°52.602′E, elevation 1363 m) where annual rainfall is >1000 mm/year (Mlingano et al., 2006). We collected 22 soil samples to a maximum depth of 177 cm using a 40 mm diameter split tube sampler (Dormer Engineering). Meru basalts have been dated between 0.059 and 2.5 million years (Bagdasaryan et al., 1973; Dawson, 1992; Wilkinson et al., 1986); however, the age of the main cone is approximately 0.050–0.38 Ma (Wilkinson et al., 1986). According to local sources, the area of soil cores has only been used for agriculture (smallholder) for no more than 3 years, the region most recently being native forest. The volcanic soils in this region were formed from a highly alkalic, augite-, plagioclase- and nepheline-bearing basaltic protolith (phono-tephrite), which was exposed approximately 100 m from the sampling site in a fresh, ~5 m deep ravine. The unweathered protolith consists of ~20% plagioclase phenocrysts (0.5–0.1 mm in diameter), set within an aphanitic groundmass made up of small phenocrysts of augite, plagioclase, occasional nepheline and Fe–Ti oxides. The resultant soils have a molic epipedon and have been formed under udic soil moisture conditions.

2.2. Bulk soil analysis

Meru soil and protolith samples were dried for 24 h at 105 °C. The water content was calculated as the mass of water lost during drying divided by mass of the dry soil. A sub-sample of the dry soil samples were heated to 550 °C for 4 h, the % mass lost reported as loss on ignition (LOI). Soil samples were taken using a split tube sampler of known volume; therefore, we made qualitative estimates of soil porosity by assuming a constant dry soil density of 2.5 g/cm^3, intended only for internal comparison. We also estimated the pH of the soil as the pH of a 1:2 mixture of dry soil and milipore water.

Aliquots of the dried samples were ground by hand with a ceramic mortar and pestle. Sample powders, a blank and BHVO1, BHVO2 and BIR1 USGS rock standards were prepared for inductively coupled plasma mass spectrometry (ICP-MS) analysis using a series of acid dissolutions at Rice University. Approximately 80 mg of the Machame soil and rock powders (BHVO1 as an external standard) were placed in Teflon beakers with ~0.5 mL each of concentrated Seastar HNO_3 and $HClO_4$. Solutions were sealed, ultrasonicated for ~20 min, heated overnight at 115 °C and subsequently dried down on heating pads at ~175 °C. This process of adding acids, overnight heating and drying down was repeated 1 additional time.

Following the second and final dry down, ~1 mL of 2% HNO_3 and ~0.1 mL of concentrated HCl were added to the samples. Beakers were ultrasonicated and then placed on a hot plate at ~100 °C for about 4 h, the samples being completely dissolved. Samples were diluted to 100 mL in polyethylene bottles using 2 wt.% HNO_3 and spiked to yield a concentration of ~1 ppb In, used to monitor instrumental drift.

All samples were run on a Finnigan Element II, single collector inductively coupled plasma mass spectrometry (ICP-MS) at Rice University in low and medium mass resolution modes ($m/\Delta m$ = 300, 4000), the latter allowing for the analysis of Na, Mg, Al, P, K, Ca, Sc, Ti, V, Cr, Mn, Fe, Co, Ni, Cu, Zn, Zr and Nb, for which isobaric molecular interferences can occasionally be a problem in low mass resolution.

A commonly used measure of the amount of chemical weathering, Chemical Index of Alternation (CIA), is calculated from the bulk chemical composition of the protolith and soils as $\mathrm{CIA} = \frac{Al_2O_3}{Al_2O_3 \cdot CaO \cdot Na_2O}$, where each of these oxides is presented as wt.% (Nesbitt and Young, 1984). The Magnesium Number (Mg#), an indicator of magmatic origin, is also calculated from the bulk chemical data as $\mathrm{Mg\#} = \mathrm{molar}\,\frac{Mg}{Mg \cdot Fe}$.

2.3. BCR (modified) extraction

A variety of extraction techniques were investigated and attempted for this study (Alloway, 1995; Asami et al., 1995; Cabral and Lefebvre, 1998; Gibson and Farmer, 1986; Han and Banin, 1995; Marin et al., 1997; Martin et al., 1987; Palumbo et al., 2000; Tessier et al., 1979). The BCR technique as reported by Marin et al. (1997) and Alloway (1995) gave the best results for our small sample sizes. Duplicate were performed for 6 of the 21 soil samples to assess reproducibility.

About 60 mg of each soil sample was accurately weighed, placed into a sealable plastic vials with ~1.5 mL of Millipore water and shaken 4 times, each for ~20 min, over the course of 24 h. The vial was shaken then centrifuged for 20 min, the supernatant removed as the water soluble fraction-centrifugation procedure was repeated 2 additional times.

Approximately 1.5 mL of an acetic acid solution (25% CH_3COOH buffered to pH 5 with CH_3COONa) was added to the undissolved residues from the previous step. The vial containing the resulting suspension was shaken 4 times, each for ~20 min, over the following 24 h. After 20 min of centrifuging. The resulting supernatant removed as the carbonate fraction.

Approximately 1.5 mL of 1 M hydroxyl amine hydrochloride solution (1 M NH_2OH–HCl in a 25% acetic acid solution) was added to vial containing the undissolved residues from the acetic acid step. The vial containing this suspension was shaken for ~30 min, 3 times over the following 24 h. The sample vial was then centrifuged for 20 min, the supernatant removed as the oxide fraction.

Undissolved residues from the previous step were washed into Teflon bottles with ~3 mL of 0.01 M HNO_3. Two milliliter of H_2O_2 was added and the bottles were placed on hot plates and heated at 80 °C until dry. Another 2 mL of H_2O_2 was added, followed again by heating at 80 °C until dry. Approximately 3 mL of 0.01 M HNO_3 was then added to the bottles and shaken. The resulting solution was removed as the organic fraction (to extract all supernatant, another 1.5 mL of H_2O was added and centrifuge procedure was repeated).

For ICP-MS analysis, the water soluble, carbonate and exchangeable, oxide and organic fractions were diluted up to 15 mL with 2% HNO_3. An In spike was added to each fraction to yield 1 ppb. Samples, procedural blanks and reference standards (BHVO1, BHVO2 and BIR1) were run on a Finnigan Element II, single collector ICP-MS at Rice University following techniques discussed above.

3. Results

3.1. Physical and chemical characteristics

The water content, loss on ignition (LOI) and porosity profiles share the same overall depth-dependant behavior (Fig. 1). The

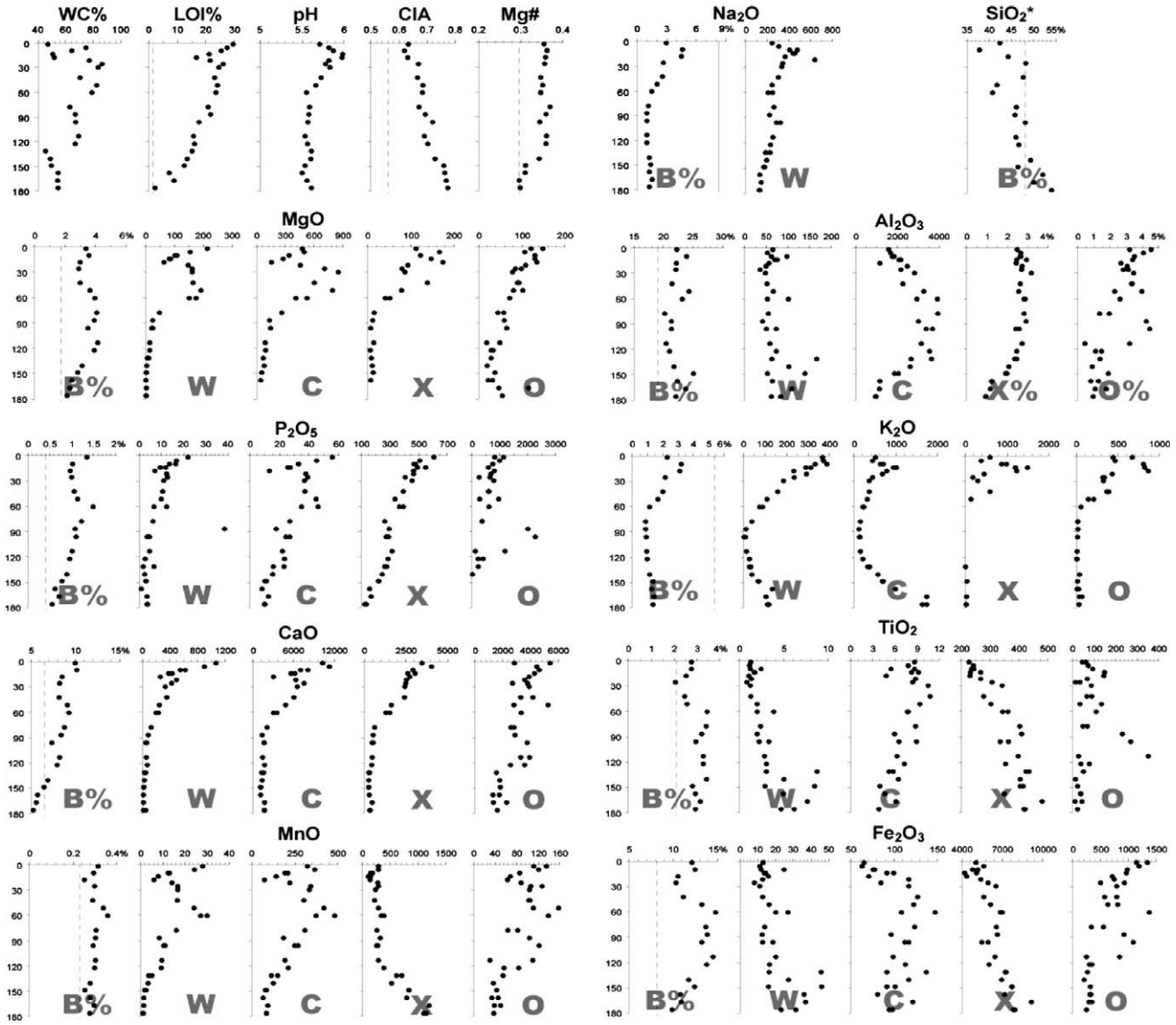

Fig. 1. *All Concentrations in ppm unless indicated on figure.* Water content (WC%), loss on ignition (LOI%), pH, chemical index of alteration (CIA) and molar Mg# $= \frac{Mg}{Mg+Fe}$ (Mg#) are plotted by depth in the first row. Bulk soil concentrations (B%) and the water soluble (W), carbonate and exchangeable (C), oxide (X) and organic (O) soil fractions of Na_2O, MgO, Al_2O_3, P_2O_5, K_2O, CaO, TiO_2, MnO and Fe_2O_3 are plotted by depth. Only the bulk and water soluble fraction of Na_2O is shown because Na was introduced in the buffered actic acid solution used for the carbonate and exchangeable step. The bulk soil composition of SiO_2 was estimated as the difference between the sum of all the major element oxide concentrations and unity. The dashed lines represent the bedrock concentrations.

water content of the soil is greater than 40 wt.% throughout the soil column (Table 1). From 2 to 26 cm, water content nearly doubles from 48% to 87%. From 26 to 61 cm, high water contents of around 80% are maintained. Between 78 and 123 cm, the water content is ~67%. The water content increases from 46% to 55% below 132 cm. The protolith's LOI is low (1%). Between 2 and 18 cm, LOI of the soil decreases from a profile-wide maximum of 29–17 wt.%. LOI increases abruptly to 26% at 26 cm and decreases steadily below to a minimum of 2% at 177 cm. The porosity also decreases between 2 and 18 cm from 81% to 75% and increases to a maximum of 82% at 26 cm. Porosity generally decreases below 26 cm, the minimum value of 70% reached at 166 cm. No significant volume increase was observed while the samples were immersed in water for the extraction procedure.

In contrast to bulk physical characteristics, the pH of the soil increases between 2 and 18 cm from 5.7 to 6.0, the maximum value. The pH decreases to 5.6 at 61 cm and remains at ~5.6 to the base of the profile. The Chemical Index of Alteration (CIA) of the protolith is 0.52. The CIA of all soil samples is greater throughout the soil and increases from ~0.6 at the surface to ~0.75 at depth. The Magnesium Number (Mg#) is ~0.35 between 2 and 141 cm but falls to protolith values of 0.30 between 149 and 177 cm.

3.2. Bulk soil composition

The bulk soil concentrations of Na, Mg, Al, P, K, Ca, Ti, Mn and Fe are reported as metal-oxides in Table 2. The bulk soil concentrations of Li, Be, Sc, Ti, V, Cr, Co, Ni, Cu, Zn, Ga, Rb, Sr, Y, Zr, Nb, Mo, Cd, Cs, Ba, La, Ce, Pr, Nd, Sm, Eu, Tb, Gd, Dy, Ho, Er, Tm, Yb, Lu, Hf, Ta, Tl, Pb, Th and U are reported online in the background dataset. Concentrations of all major element oxides and Sr, Ba and La are plotted against depth in Fig. 2.

Na_2O, K_2O and Rb are all depleted near the surface (~50%) but more depleted below 61 cm (~80%). Cs also decreases with depth from near-protolith values above 61 cm to 50% depletions below. Li generally decreases with depth; but Li is enriched over the

Table 1
Bulk physical properties.

%	2 cm	10	18	26	43	52	61	78	87	96	114	123	141	149	158	167	177	Prot	LOD
WC	48	65	52	87	71	83	79	63	67	67	70	67	49	50	55	54	55		
LOI	29	25	17	26	23	24	23	21	22	18	16	16	13	12	7	9	2	1	
Porosity	81	79	75	82	78	81	81	78	77	77	79	76	72	72	73	70	71		
pH	5.7	5.9	6	5.8	5.7	5.7	5.6	5.6	5.6	5.6	5.5	5.6	5.6	5.5	5.5	5.6	5.6		

Water content (WC), loss on ignition (LOI), porosity and pH are reported. WC is the percent of the bulk soil lost after 12 h at 105 °C; LOI is the percent of dry soil lost after 4 h at 550 °C; and porosity was approximated, porosity $= 1 - \frac{V_{\text{Total}} * M_{\text{dry soil}}}{\rho_{\text{drysoil}}}$ assuming $\rho_{\text{drysoil}} = 2.5\,\text{g/cc}$.

Table 2
Bulk major element chemical properties.

Na_2O	3.72	5.8	5.66	3.35	3.26	2.54	1.84	1.44	1.26	1.22	1.23	1.25	1.54	1.77	1.54	1.9	1.54	10.45	0.00015
MgO	3.38	3.59	2.99	2.89	3.02	3.64	3.97	4.07	3.93	3.52	4.15	3.93	3.12	2.85	2.46	2.34	2.13	1.72	0.00014
Al_2O_3	22.36	23.98	22.22	22.14	21.48	24.37	23.22	20.28	21.44	21.4	20.52	21.06	21.86	25.1	22.45	23.8	22.21	19.12	0.001
P_2O_5	1.36	1.03	0.97	1.01	1.06	1.14	1.5	1.23	1.08	1.1	1.02	0.96	0.89	0.78	0.62	0.71	0.56	0.41	0.00011
K_2O	2.4	3.35	3.26	2.26	2.1	1.77	1.21	0.94	0.93	0.97	1.01	1.05	1.2	1.43	1.34	1.5	1.42	5.63	0.0053
CaO	10.69	10.87	9.1	8.81	8.77	9.77	9.95	9.39	9.04	7.9	8.82	8.51	7.44	6.96	6.17	6.02	5.64	7	0.002
TiO_2	2.76	2.77	2.53	2.06	2.47	2.58	3.45	3.39	3.2	2.95	3.27	3.28	3.42	2.81	2.94	3.15	2.94	2.09	0.00014
MnO	0.31	0.29	0.25	0.3	0.29	0.34	0.36	0.31	0.3	0.29	0.3	0.3	0.28	0.26	0.28	0.3	0.28	0.23	7.4E−06
Fe_2O_3	12.13	12.47	10.55	10.31	11.17	13.25	14.78	13.71	13.82	13.22	14.5	13.77	11.75	12.42	10.81	10.92	9.9	8.11	0.00059
SiO_2[a]	41	36	42	47	46	41	40	45	45	47	45	46	49	46	51	49	53	45.24	
CIA	0.61	0.59	0.6	0.65	0.64	0.66	0.66	0.65	0.68	0.7	0.67	0.68	0.71	0.74	0.74	0.75	0.76	0.52	
Mg#	0.36	0.36	0.36	0.36	0.35	0.35	0.35	0.37	0.36	0.35	0.36	0.36	0.34	0.31	0.31	0.30	0.30	0.30	

All soil concentrations determined using medium resolution ICP-MS and protolith (Prot) concentrations using XRF. The Chemical Index of Alteration (CIA) is defined as $\text{CIA} = \frac{Al_2O_3}{Al_2O_3 \cdot CaO \cdot Na_2O}$ and the molar Mg number (Mg#) is defined as$\text{Mg\#} = \text{molar}\,\frac{Mg}{Mg \cdot Fe}$.
[a] SiO_2 soil concentrations were estimated as the difference between the sums of the major element oxides for each soil sample.

protolith concentrations by ~30% above 61 cm and hovers around the protolith concentration below.

Between 2 and 96 cm, MgO and CaO are enriched over protolith values by 100 and 40%, respectively. Both subsequently decrease below 96 cm, approaching a protolith concentration below 150 cm. In contrast, the other alkaline metals are not generally enriched, nor do they exhibit an overall trend similar to MgO and CaO. Be concentrations are equivalent to the protolith throughout the profile. Sr is depleted by ~20% at the top and bottom of the profile and by more than 100% in the middle. Ba is depleted by >20% from the surface down to 123 cm. Below 123 cm, Ba is enriched.

MnO and Fe_2O_3 are enriched moderately throughout the profile and up to 50% at 2 cm and between 52 and 123 cm. TiO_2 is also moderately enriched down to 52 cm; but, the greatest enrichment is below 61 cm (>50%). The other period 4 transition metals, Sc, V, Cr, Co, Ni and Zn, are also enriched throughout the profile and behave most like Fe_2O_3. The lowest concentrations of these metals are found at or near the bottom of the soil profile and the highest concentrations are found at 61 and 114 cm where these maxima represent 2–10-fold enrichments relative to the protolith. Cu is also enriched throughout the profile by more than 300%, but Cu does not show any dynamic behavior with depth.

Al_2O_3 is consistently enriched relative to the protolith by ~10% in all soil samples. Ga, Y, Zr, Nb, the REE's (La, Ce, Pr, Nd, Sm, Eu, Tb, Gd, Dy, Ho, Er, Tm, Yb and Lu), Hf, Ta, U, Th and Pb are enriched by 10 to 30% over the protolith concentrations. In general, REE's are constant with depth though higher REE concentrations are found in deeper samples. There appears to be no fractionation between the light, medium and heavy REE's; however, there is a negative Ce anomaly in most samples, a negative Eu anomaly in all samples and a positive Gd anomaly in all samples relative to the protolith.

P_2O_5 is enriched throughout the profile and generally decreases with depth; however, enrichments at the surface and at 61 cm are greater than any other major element (>200% enrichment). Soil Tl is enriched throughout the soil profile and, in general, increases with depth.

Changes in the concentrations of Al, Ti, Zr, Nb, Hf and Ta, the least mobile elements in the bedrock and soil, should reveal any bulk mass losses or gains (Brimhall et al., 1991, 1988; Chadwick et al., 1990; Kurtz et al., 2000; Little and Lee, 2006; Melfi et al., 1996; Sak et al., 2003; Sastri and Sastry, 1982; Taylor and Blum, 1995; Teutsch et al., 1999). If any two of these elements were perfectly immobile, their ratio would be constant throughout the soil and bedrock protolith. In Fig. 4A, Zr/Hf ratios for the soil plot on the protolith-origin line, suggesting that Zr and Hf are relatively immobile in the Meru soils (element–element ratios of Al, Ti, Nb and Ta also plot close to the protolith-origin line). The net (%) mass loss/gain, $\Delta Mass$, can be estimated from the soil/protolith ratios of any of these immobile elements, i.e. $\Delta Mass = 100 * \left(\frac{C^i_{\text{protolith}}}{C^i_{\text{soil}}} - 1\right)$, where $\frac{C^i_{\text{protolith}}}{C^i_{\text{soil}}}$ is the protolith/soil ratio of any immobile element, *i*. In Fig. 4B, we plot the $\Delta Mass$ calculated from Al, Ti, Zr, Nb, Hf and Ta. Zr, Hf, Al and Ta all predict approximately 10–30% mass losses throughout the profile. Ti and Nb behave slightly differently: Ti predicts mass losses >40% between 61 and 141 cm and Nb predicts mass *gains* between 2 and 123 cm. Given the consistent behavior of Zr, Hf, Al and Ta and the well-behaved Zr/Hf ratios, we use Zr to calculate mass losses throughout the soil column.

In Fig. 4C, we plot the concentration ratios of soil to protolith averaged over the top 114 cm. The dashed line, which passes through the Zr soil/protolith ratio, represents the maximum enrichment that can be achieved by a perfectly conservative (immobile) element during chemical weathering. The soil/protolith ratios of many elements, most notably the REEs, fall on this line. However, Mg, P, Ca, Ti, Mn and Fe ratios fall above the Zr line.

3.3. Sequential extractions

The composition of the water soluble, carbonate and exchangeable, oxide, and organic extractions are reported online in the background data set. Concentrations of the major elements and selected minor elements are plotted in Figs. 1 and 2. Water soluble concentrations of all elements are very low ($\geqslant$3 orders of magnitude below bulk) and generally decrease with depth with the exception of the refractory elements, Ti, Fe, etc., which show mod-

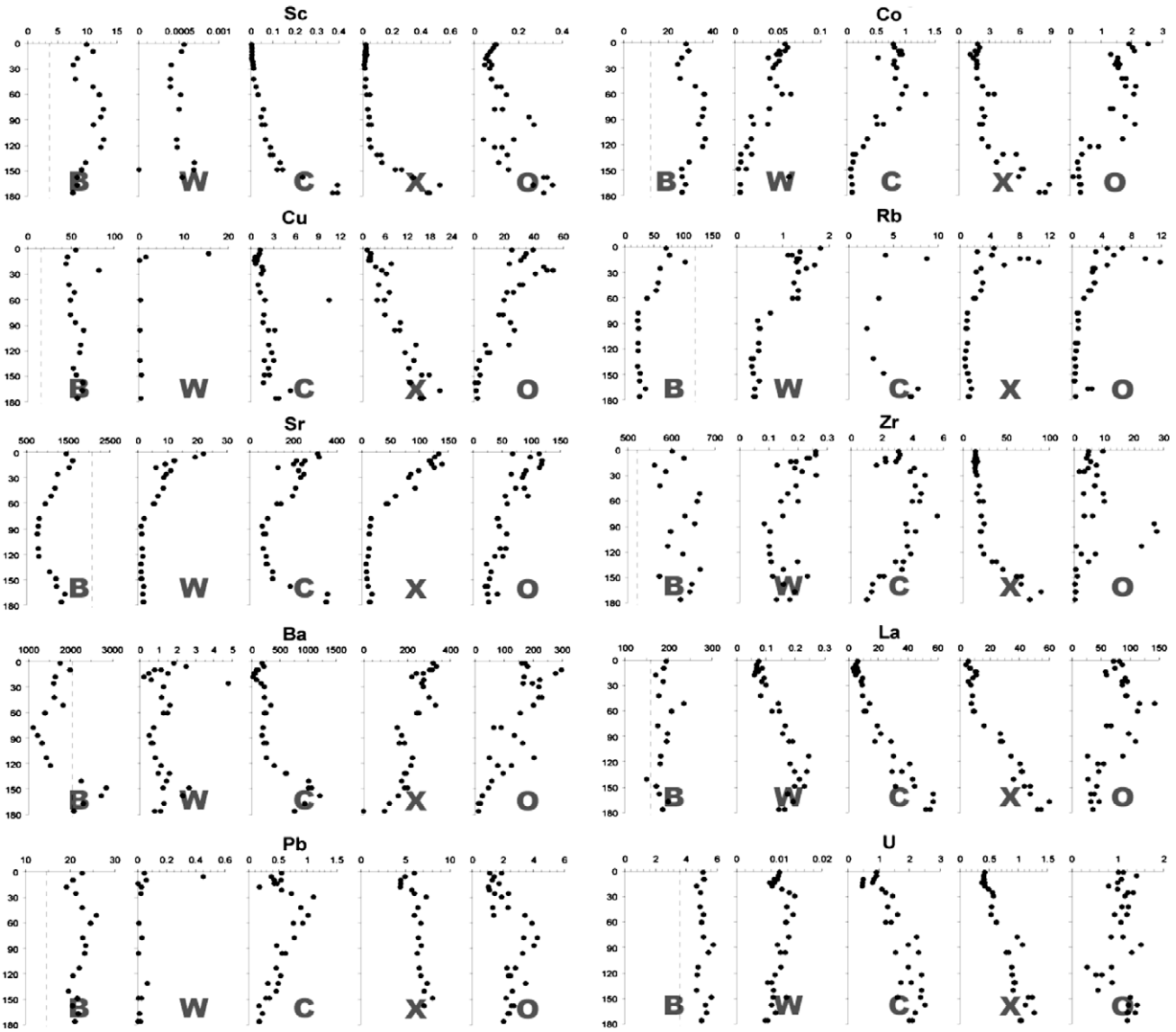

Fig. 2. *All Concentrations in ppm.* Bulk soil concentrations (B) and the water soluble (W), carbonate and exchangeable (C), oxide (X) and organic (O) soil fractions of Sc, Co, Cu, Rb, Sr, Zr, Ba, La, Pb and U are plotted by depth. All REE's generally behave like La. The dashed lines represent the bedrock concentrations.

erate increases with depth. The fractions of select elements released in the carbonate and exchangeable, oxide and organic extractions are shown in Fig. 3.

The carbonate and exchangeable fraction was, generally, ~2 orders of magnitude below the bulk soil concentrations. More than 1% of bulk K_2O was released in this step. Both K_2O and Cs display a strong surface depletion down to 14 cm juxtaposed on a C-shaped profile with significant increase below 132 cm. Li is fairly constant with depth except for some high outliers between 132 and 149 cm. MgO and CaO both display a shallow, 18 cm deep, surface depletion juxtaposed on a profile that generally decreases with depth. Sr is similar, but increases in concentration below 132 cm and is >10% of the bulk Sr throughout the profile. Be and Ba are both fairly constant between 2 and 114 cm, but increase significantly below 114 cm. Ba in the carbonate and exchangeable extraction represents up to 30% of the bulk soil Ba.

Sc, Cu, Y, Ga and REE's generally increase with depth in the carbonate and exchangeable fraction with Sc approaches 10% of the bulk soil concentrations at the base of the profile. As for the REE's, there is a clear negative Ce anomaly in all samples, a strong positive Eu anomaly in the shallow samples and a slight negative Eu anomaly in the deep samples. Fe_2O_3, Tl and U also increase with depth with more than >20% of bulk Tl and U is released. Al_2O_3, Zr, Hf and Th increase between 2 and 52 cm and decrease below 132 cm.

The oxide fraction is, generally, 2–3 orders of magnitude below the bulk soil with some significant exceptions. K_2O and Rb are both surface enriched, the latter comprising ~10% of the bulk soil concentration. Li also decreases with depth, but increases below 114 cm. MgO, CaO, Sr and Ba tend to behave like the alkali metals. More than 50% of total Be is released in the oxide leach. The concentrations of MnO, TiO_2, Fe_2O_3, Sc, V, Co, Cu, Zr, Nb, Hf, Pb, Th and U increase with depth—between 1% and 10% of the bulk soil MnO, Fe_2O_3, Co, Nb and Zr and as much as 10–30% of bulk soil V, Cu, Pb and U are released in the oxide leach. Y and the REE's tend to increase continually with depth in the oxide fraction which constitutes ~1% of the bulk soil concentrations. There is also a significant negative Ce anomaly in all samples and a negative Eu anomaly in some samples. Oxide fraction concentrations of Al_2O_3, P_2O_5 and Zn all decrease with depth and represent ~10% of the bulk soil. Approximately 10% of bulk Ga is in the oxide leach.

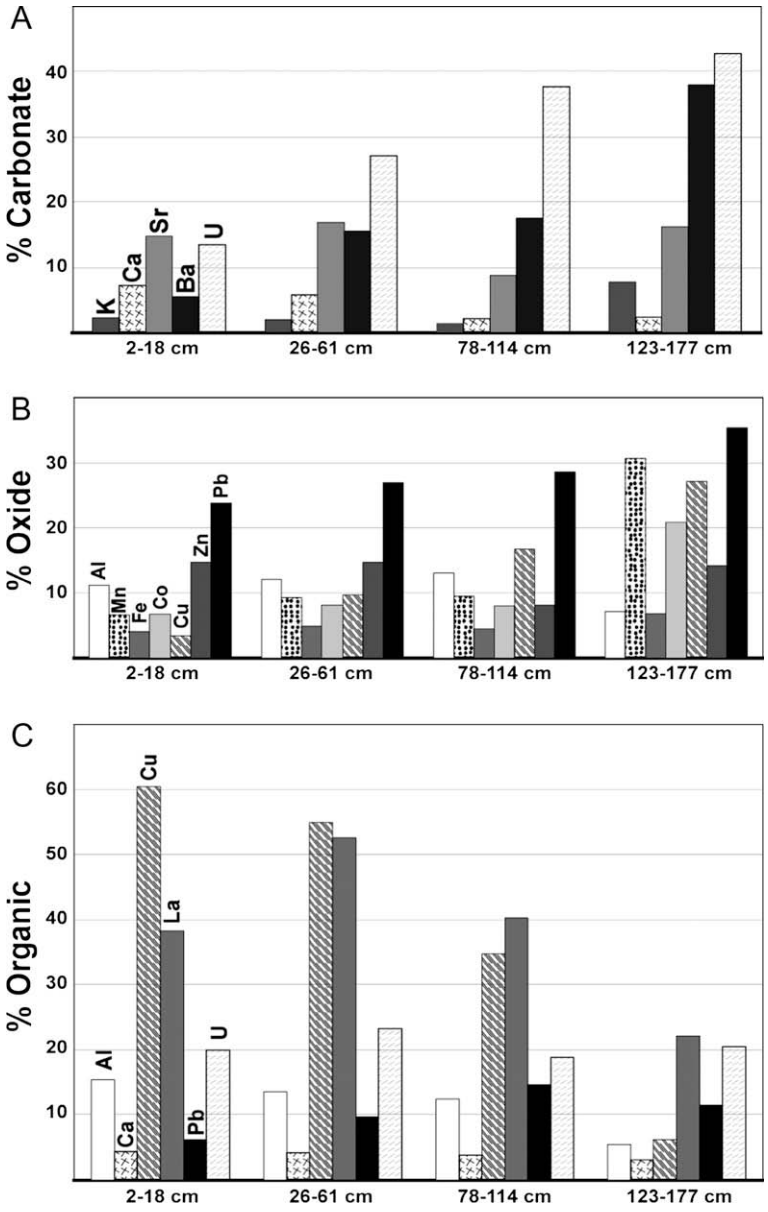

Fig. 3. Percentage of bulk soil K, Ca, Sr, Ba and U in the carbonate extraction [A]. Percentage of Al, Mn, Fe, Co, Cu, Zn and Pb in the oxide extraction [B]. Percentage of Al, Ca, Cu, La, Pb and U in the organic extraction [C]. All percentages were averaged over the depth ranges indicated on the plot.

The organic extraction removed 1–10% of the bulk alkali metals, K_2O, Li, Rb and Cs, all decreasing with depth in this step. Most of the alkaline metals, MgO, CaO, Sr and Ba, also decrease with depth. While MgO and Ba concentrations are quite low, ~3% of bulk CaO and nearly 10% of Sr is released in the organic step. More than 10% of total Be is also released; however, the data is scattered. Most of the other elements analyzed also generally decreased with depth: Al_2O_3, P_2O_5, TiO_2, MnO, Fe_2O_3, Co, Ni, Cu, Zn and Ga. ~10% of the bulk soil Al_2O_3, P_2O_5, Ni, Zn and Ga and nearly 50% of bulk Cu are released in the organic leach. Organic TiO_2 falls 3 orders of magnitude below the bulk soil and only ~1% of bulk MnO, Fe_2O_3 and Co were recovered herein. About 1% of Zr, Nb, Y, REE's, Hf, Ta and Th are released in the organic leach though as much as ~30% of the bulk REE's are released. Samples below 149 cm have a negative Ce anomaly and all other samples have clear positive Ce anomalies. All samples show a clear a negative Eu anomaly in the organic leach. Only Sc and Pb increase with depth in the organic leach with more than 10% of total Pb released in the organic step.

4. Discussion

4.1. Surface-enrichments in the bulk soil

The elemental concentrations of bulk soil profiles are characterized by enrichments at the surface relative to deeper sections of the soil profile. In many cases, elemental concentrations are even higher than that of the protolith. There are two ways to achieve these concentration enrichments: (1) selective removal of soluble elements during chemical weathering concentrates immobile or refractory elements retained in the soil residue, or (2) external inputs, such as atmospheric deposition, re-enrich the soil column. As shown in Fig. 4C, major elements Mg, P, Ca, Ti, Mn and Fe are all enriched relative to Zr and Hf; therefore, enrichments in these elements cannot be solely explained by the concentrating effects of mass loss on conservative elements during soil formation.

We now return to the zoned elemental profiles in the soil column. It can be seen in Fig. 4C that most element enrichments are

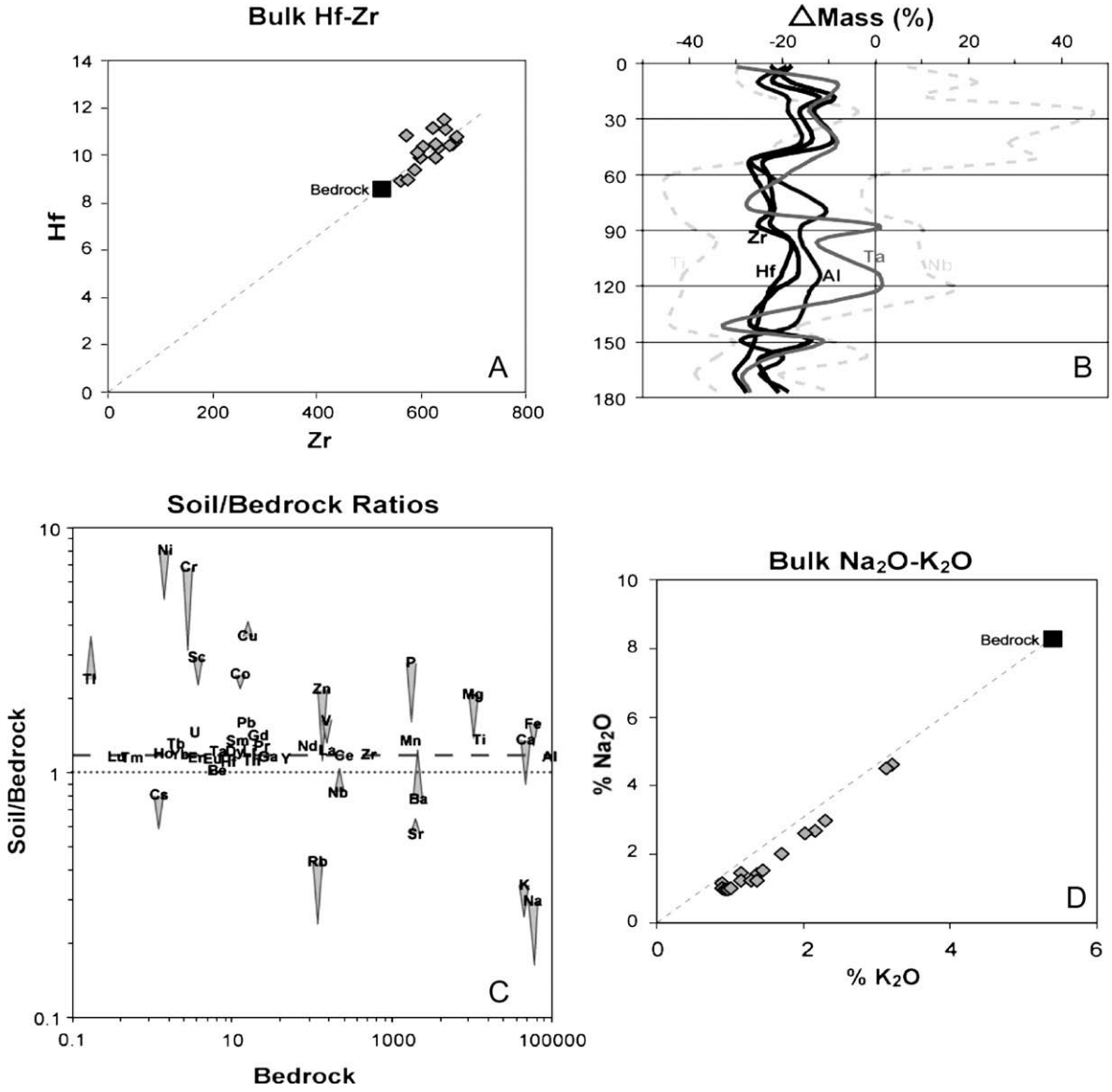

Fig. 4. *All concentrations in ppm unless indicated on figure.* Hf/Zr ratios throughout the bulk soil (♦) and bedrock (■) are consistent [A]. Our estimate of the % Δ*Mass* of the soil is calculated from soil/bedrock ratios of Al, Ti, Zr, Nb, Hf and Ta [B]. Soil/Bedrock ratios averaged over the upper 114 cm are plotted for all elements [C]. The dotted line runs through a soil/bedrock ratio of 1 representing immobile elements assuming no mass loss. The dashed line runs through the soil/bedrock ratio of Zr, 1.18, representing immobile elements relative to Zr. The termini of the gray triangles represent soil/bedrock ratios averaged over samples below 150 cm. Na_2O/K_2O ratios throughout the bulk soil (♦)and bedrock (■) are also consistent [D].

confined to the upper 114 cm, which is the reverse of that expected for typical soil profiles where the shallowest samples tend to be the most weathered and hence most depleted in soluble elements. The decrease in soil/protolith ratio for many soluble elements is denoted by the endpoints of the gray triangles representing the average soil/protolith ratio *below* 150 cm. We also note that the Mg# of the bulk soil also follows a reverse depth zonation. It is high at depths shallower than 114 cm but similar to the protolith deeper than 150 cm. Collectively, these observations suggest that the soil shallower than 114 cm was formed from or contains a significant component of materials, which are higher in Mg, P, Ca, Ti, Mn and Fe relative to the weathered soil residue at depth.

There are a number of ways to explain these surface enrichments. They could (1) be artifacts of a layered or heterogeneous protolith or (2) derive from surface-deposited material external to the present-day soil column (Capo and Chadwick, 1999; Chadwick et al., 1999). Another possibility is that this soil profile represents an inverted weathering column, wherein the lower part is more deeply weathered due to enhanced weathering associated with subsurface water flow (Little and Lee, 2006). The subsurface water flow scenario was proposed by Little and Lee (2006) for a lateralized soil column on the slopes of Mt. Kilimanjaro, just east of Mt. Meru. However, in that study, there was a substantial increase in immobile elements (Zr, Hf, Nb, Ta) with depth, corresponding to enhanced mass loss at depth. The lack of any significant variation in immobile elements with depth in the Meru site suggests that there are probably not strong depth zonations in the degree of chemical weathering in the present study, so the subsurface water flow scenario is not applicable to the Meru site.

Thus, only the first two hypotheses are likely to pertain to the Meru site. While we have no means of ruling out a heterogeneous protolith, a number of observations seem to require some addition of a foreign soil component, such as dust. Na and K increase towards the surface yet Na_2O/K_2O ratios are constant throughout

the soil and protolith despite major changes in bulk soil composition (Fig. 4D). Given the high solubility of Na and K, it seems highly unlikely that Na and K can be elevated at shallow depths and that the Na/K ratio can remain constant in soil residues. This dilemma can be resolved if the shallow soil had been "re-fertilized" by less weathered materials with higher Na and K and similar Na/K ratios as the protolith itself. One possibility could be the addition of dust in the form of juvenile volcanic ash from one of the newer cones on Mt. Meru. Such a scenario would also be consistent with the enrichments in Ni and Mg towards the surface. These elements might be expected to be leached out during chemical weathering, but they could be re-enriched if fresh volcanic ash (e.g., unweathered) had been introduced. In the following sections, we discuss the processes, which may control the behavior and distribution of elements within the soil column.

4.2. Carbonate and exchangeable fractions

The two most salient characteristics of the carbonate and exchangeable fraction are the role carbonates play in the sequestration of labile Sr, Ca Ba and U (Fig. 3A) and the relative behavior of these elements (Fig. 5). Ca and Mg are the most abundant carbonate-forming cations in our soils and they both decrease with depth in the bulk and carbonate fraction. However, B and U increase with depth; more than 15% of Sr and more than 35% of both Ba and U are found in the carbonate fraction at depth; and changes in Sr/CaO ratios below 114 cm indicate that the composition of the carbonate present changes significantly (Fig. 2).

Because of similar electrochemical behavior Sr/CaO ratios can be used to track the sources of Ca in natural systems because Ca and Sr are often incorporated into the same minerals (Blum et al., 2002). The bulk soil Ca and Sr are not correlated; however, in the carbonate and exchangeable fraction, Sr/Ca ratios are correlated (Fig. 5A). The carbonate fraction of soil samples above 123 cm and the protolith share the same Sr/CaO ratio; however, the ratio changes drastically below 114 cm suggesting a change in the Sr/CaO ratio of the carbonate minerals being formed at these depths. This change in Sr/CaO is unique to the carbonate and exchangeable step: the Sr/CaO ratio of the water soluble and oxide fractions do not deviate from the protolith ratio (Fig. 5B). Like Sr and Ca, Ba also occurs as a divalent cation that forms weakly soluble carbonates in nature (Sulkowski and Hirner, 2006; Velde, 1992). Ba/CaO behaves like Sr/CaO in the carbonate and exchangeable (Fig. 5C). However, below 114 cm, the Ba/CaO ratio of the soil increases dramatically such that >30% of the bulk Ba is in carbonate at these depths (Figs. 5a and 6c).

Carbonate and exchangeable Sc increases exponentially with depth, such that the greatest change in concentration occurs below

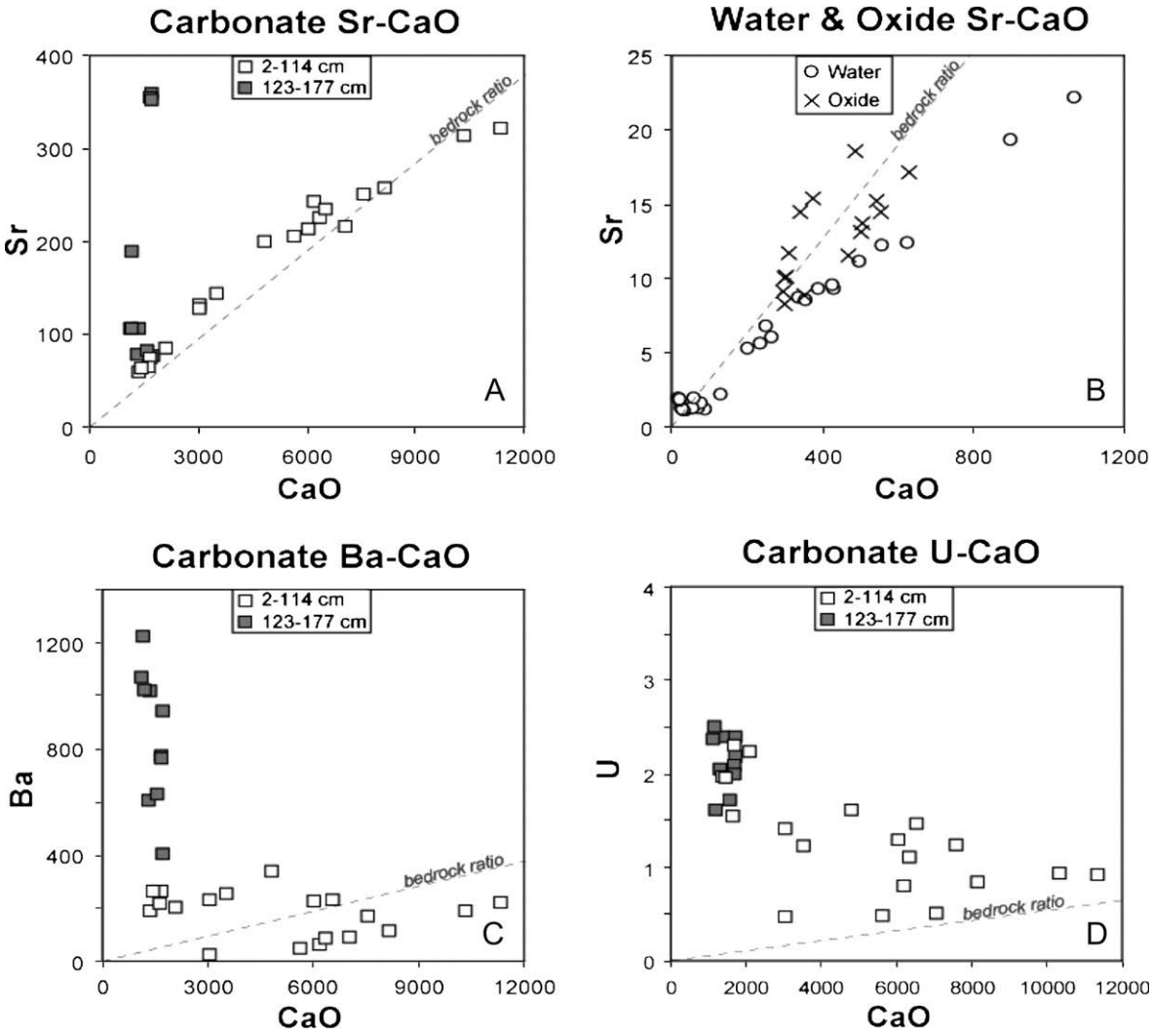

Fig. 5. *All concentrations in ppm.* Sr/CaO in the shallow (2–114 cm) soil (□) and bedrock (dashed line) are consistent; however deep (123–177 cm) samples (■) differ [A]. Both water soluble (○) and oxide (X) Sr/CaO ratios are consistent with the bedrock throughout the soil column [B]. Ba/CaO in the shallow soil and bedrock are consistent; however deep samples differ [C]. U does not correlate well with any element, though U/CaO ratios do tend to higher below 123 cm.

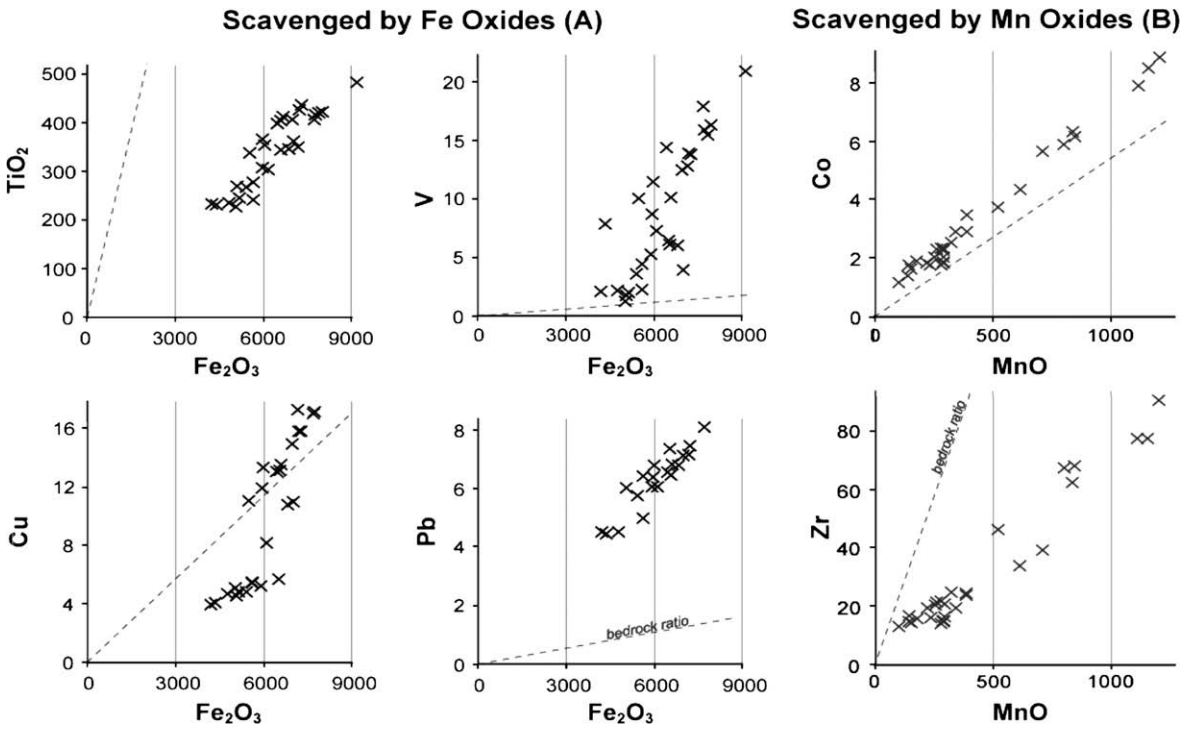

Fig. 6. *All concentrations in ppm.* TiO_2, V, Cu and Pb linearly correlate with Fe_2O_3 in the oxide fraction [A]. Co and Zr correlate with MnO [B]. The bulk bedrock ratio of these elements is plotted as a dashed line.

114 cm while the REE's, represented by La, increase linearly with depth (Fig. 2). U increases more abruptly such that below 78 cm, >35% of bulk U in the bulk soil is in the carbonate (Fig. 3A). Neither Sc, the REE's nor U correlate with CaO (Fig. 5D), but below 114 cm, high concentrations of carbonate and exchangeable K, Sr, Ba, Sc, REE's and U are available.

4.3. Scavenging of metals by metal hydroxides

More than 10% of bulk Al, Fe and Mn are released in the oxide fraction indicating the presence of metal hydroxides and oxyhydroxides common to highly weathered tropical soils (Alloway, 1995). Al-oxides do not effectively scavenge other elements; however in Fig. 6, we show positive correlations of Ti, V, Cu and Pb with Fe and Co and Zr with Mn, consistent with reported Fe and Mn oxide scavenging behavior (Alloway, 1995; Keller and Vedy, 1992; Teutsch et al., 1999). This positive, linear correlation implies that increases in Fe or Mn oxides will result in the absorption and hence retention of labile Ti, Cu, V, Pb, Co or Zr. Although Ti and Fe and Zr and Mn are highly correlated, the soil ratios, TiO_2/Fe_2O_3 and Zr/MnO, are low compared to the protolith value (Fig. 6). The relatively immobile behavior of Ti and Zr most likely contributes to their low availability in a labile form during soil formation. The high ratios of Cu, Co, V and Pb relative to Fe and Mn in the oxides indicates higher availability of these elements for absorption. These elements are mobilized during chemical weathering, but some fraction is re-immobilized by absorption onto Fe–Mn-oxyhydroxides.

A feature of interest is where the regression line of a given metal versus Fe or Mn intercepts. Most of the elements (Pb, Co, Ti, Zr) plotted against Fe or Mn (Fig. 6) have regressions that go through the origin or just slightly above the origin. These elements are probably quantitatively adsorbed by Fe–Mn oxyhydroxides. In contrast, the Cu and V versus Fe_2O_3 regressions intercept the *y*-axis (Cu or V) at negative values, which implies that although these elements are scavenged by Fe–Mn oxyhydroxides, they are probably not as efficiently scavenged as Pb, Co, Ti and Zr.

4.4. Metals in the organic fraction

A large fraction of the bulk Al_2O_3, Cu, La (REE's), Pb and U was released in the organic extraction (Fig. 3C). The presence of Al-organic complexes above 123 cm could explain why >10% of the bulk Al_2O_3 is released in the organic step (Fig. 3C). Such complexes were found to be a significant pool of Al in soils with a similar pH (~5.5) formed from volcanic ash in France (Prevosto et al., 2004). Bulk soil enrichments of Cu and Pb are often associated with organic matter and most of the bulk enrichment of Cu above 123 cm and of Pb below 26 cm can be accounted for in the organic fraction (Alloway, 1995; Gibson and Farmer, 1986; Keller and Vedy, 1992; Palumbo et al., 2000; Rahman et al., 1996; Teutsch et al., 1999). REEs are relatively immobile thus we did not expect to find >50% of the bulk soil REEs in the organics (Fig. 3C); however, the capacity of organic coatings to absorb REEs in seawater has been demonstrated, thus it is reasonable that a significant portion of REEs are incorporated into organic matter (Byrne and Kim, 1990).

The organic fraction duplicates for all elements analyzed are less consistent than the oxide, carbonate and exchangeable, water soluble and bulk fractions (Figs. 2 and 3). The inconsistent solubilization of the organic-bound soil fraction, the oxidation of sulfides by H_2O_2, or the solubilization of some clay minerals may all contribute to the scatter (Keller and Domergue, 1996; Marin et al., 1997; Sulkowski and Hirner, 2006; Tessier et al., 1979).

5. Conclusions

Unlike population trends in Europe, East Asia and the Americas, rural areas in East Africa continue to share a significant portion of the population growth. As small holder farming supplies the bulk of foodstuffs in these areas, fertile soil will continue to be

exploited—including volcanic soils in the mountainous northern region of Tanzania. Our study shows that, despite a predicted total mass loss of 10–30% during pedogenesis from rock to soil, major and minor elements important to plant growth – P, Mg and Ca—are enriched. The apparent enrichments of P, Mg and Ca, as well as Ti, Mn, Fe and some minor elements, are most likely caused by volcanic ash deposition or are inherited from a heterogeneous parent lithology. However, parent lithology alone cannot explain why elements are enriched in the labile fraction, e.g., K in layers above 30 cm and below 114 cm; Ca in carbonates above 61 cm; and both Sr and Ba in carbonates below 114 cm.

In addition to these elements, some necessary for plant growth, these soils also contain labile heavy metals which are potentially unhealthy for human consumption. While the majority of total Cu and ~5–10% of bulk Pb that are associated with the organic fraction and may be practically immobile under normal agricultural conditions, a significant presence of Fe and Mn oxides indicates a capacity of these soils to sequester heavy metals. At some depths, more than 5% of total Fe and 30% of total Mn are in the oxide fraction. Moreover, Fe and Mn oxides are effective at scavenging 20–30% of total Co, Cu and Pb below 114 cm. The presence and amount of these oxides also indicates their potential as a significant reservoir for additions of these metals from the future use petroleum, fertilizers or other anthropogenic sources.

Based on the behaviors of both major elements necessary for plant growth and minor elements potentially unhealthy for human consumption, significant labile element reservoirs exist throughout the soil column in phases with different levels of mobility.

Acknowledgments

We thank A.S.S. Mbwana, Rama Ngatoluwa and George Sayulla of the Selian Research Institute in Arusha, Tanzania for their support. We are also grateful to Musa Naroro, Felix John and Nuru for logistical help in the field. Conversations with Glen Snyder and David J. Brown were instructive. Comments by Jacques Etame and an anonymous reviewer were invaluable. This work was supported by a Ford Foundation fellowship to Little and Rice University startup funds and a Packard fellowship to Lee.

Appendix A. Supplementary material

Supplementary data associated with this article can be found, in the online version, at doi:10.1016/j.jafrearsci.2009.12.001.

References

Alloway, B.J., 1995. Heavy Metals in Soils, Heavy Metals in Soils. Blackie Academic and Professional, Suffolk, England. 368 pp.
Asami, T., Kubota, M., Orikasa, K., 1995. Distribution of different fractions of cadmium, zinc, lead and copper in unpolluted and polluted soils. Water, Air, & Soil Pollution 83, 187–194.
Bagdasaryan, G.P., Gerasimovskiy, V.I., Polyakov, A.I., Gukasyan, R.K., Vernadskiy, V.I., 1973. Age of volcanic rocks in the rift zones of East Africa. Geochemistry International 10, 66–71.
Blum, J.D., Klaue, A., Nezat, C.A., Driscoll, C.T., Johnson, C.E., Siccama, T.G., Eagar, C., Fahey, T.J., Likens, G.E., 2002. Mycorrhizal weathering of apatite as an important calcium source in base-poor forest ecosystems. Nature 417, 729–731.
Boko, M., Niang, I., Nyong, A., Vogel, C., Githeko, A., Medany, M., Osman-Elasha, B., Tabo, R., Yanda, P., 2007. Africa climate change 2007: impacts, adaptation and vulnerability. In: Parry, M.L., Canziani, O.F., Palutikof, J.P., van der Linden, P.J., Hanson, C.E. (Eds.), Contribution of Working Group II to the Fourth Assessment Report of the Intergovernmental Panel on Climate Change. Cambridge University Press, Cambridge UK, pp. 433–467.
Brimhall, G.H., Chadwick, O.A., Lewis, C.J., Compston, W., Williams, I.S., Danti, K.J., Dietrich, W.E., Power, M.E., Hendricks, D., Bratt, J., 1991. Deformational mass transport and invasive processes in soil evolution. Science 255, 695–702.
Brimhall, G.H., Lewis, C.J., Ague, J.J., Dietrich, W.E., Hampel, J., Teague, T., Rix, P., 1988. Metal enrichment in bauxites by deposition of chemically mature aeolian dust. Nature 333, 819–824.
Byrne, R.H., Kim, K.-H., 1990. Rare earth element scavenging in seawater. Geochimica et Cosmochimica Acta 54, 2645–2656.
Cabral, A.R., Lefebvre, G., 1998. Use of sequential extraction in the study of heavy metal retention by silty soils. Water, Air, & Soil Pollution 102.
Capo, R.C., Chadwick, O.A., 1999. Sources of strontium and calcium in desert soil and calcrete. Earth and Planetary Science Letters 170, 61–72.
Chadwick, O.A., Brimhall, G.H., Hendricks, D.M., 1990. From a black to a gray box – a mass balance interpretation of pedogenesis. Geomorphology 3, 369–390.
Chadwick, O.A., Derry, L.A., Vitousek, P.M., Huebert, B.J., Hedin, L.O., 1999. Changing sources of nutrients during four million years of ecosystem development. Nature 397, 491–497.
Dawson, J.B., 1992. Neogene tectonics and volcanicity in the Noth Tanzania sector of the Gregory Rift Valley: contrasts with the Kenya sector. Tectonophysics 204, 81–92.
Gibson, M.J., Farmer, J.G., 1986. Multi-step sequential chemical extraction of heavy metals from urban soils. Environmental Pollution Series B 11, 117–135.
Han, F., Banin, A., 1995. Selective sequential dissolution techniques of potentially toxic heavy metals in arid-zone soils: the carbonate dissolution step. Communications in Soil Science and Plant Analysis 26, 553–576.
Kaizzi, K.C., Byalebeka, J., Wortmann, C.S., Mamo, M., 2007. Low input approaches for soil fertility management in semiarid eastern Uganda. Agronomy Journal 99, 847–853.
Keller, C., Domergue, F.-L., 1996. Soluble and particulate transfers of Cu, Cd, Al, Fe and some other major elements in gravitational waters of a Podzol. Geoderma 71, 263–274.
Keller, C., Vedy, J.-C., 1992. Distribution of copper and cadmium fractions in two forest soils. Journal of Environmental Quality 23, 987–999.
Kurtz, A.C., Derry, L.A., Chadwick, O.A., Alfano, M.J., 2000. Refractory element mobility in volcanic soils. Geology 28 (8), 683–686.
Little, M.G., Lee, C.-T.A., 2006. On the formation of an inverted weathering profile on Mount Kilimanjaro, Tanzania: buried paleosol or groundwater weathering? Chemical Geology 235, 205–221.
MacIntyre, R.M., Dawson, J.B., Mitchell, J.G., 1974. Age of fault movements in Tanzanian sector of the East African rift system. Nature 247, 354–356.
Marin, B., Valladon, M., Polve, M., Monaco, A., 1997. Reproducibility testing of a sequential extraction scheme for the determinaiton of trace metal speciation in a marine reference sediment by inductively coupled plasma-mass spectrometry. Analytica Chimica Acta 342, 91–112.
Martin, J.M., Nirel, P., Thomas, A.J., 1987. Sequential extraction techniques: Promises and problems. Marine Chemistry 22, 313–341.
Mati, B. 2005. Overview of Water and Soil Nutrient Management Under Smallholder Rainfed Agriculture in East Africa. IWMI Working Paper 105. IWMI, Colombo, Sri Lanka.
Melfi, A.J., Subies, F., Nahon, D., Formoso, M.L.L., 1996. Zirconium mobility in bauxites of Southern Brazil. Journal of South American Earth Sciences 9 (3/4), 161–170.
Mlingano Agricultural Research Institute, 2006. Rainfed Agriculture Crop Suitability for Tanzania, Mlingano Agricultural Research Institute, Tanga, Tanzania.
Nesbitt, H.W., Young, G.M., 1984. Prediction of some weathering trends of plutonic and volcanic rocks based on thermodynamic and kinetic considerations. Geochimica et Cosmochimica Acta 48, 1523–1534.
Palumbo, B., Angelone, M., Bellanca, A., Dazzi, C., Hauser, S., Neri, R., Wilson, J., 2000. Influence of inheritance and pedogenesis on heavy metal distribution in soils of Sicily, Italy. Geoderma 95, 247–266.
Potts, D., 2009. The slowing of sub-Saharan Africa's urbanization: evidence and implications for urban livelihoods. Environment and Urbanization 21 (1), 253–259.
Prevosto, B., Dambrine, E., Moares, C., Curt, T., 2004. Effects of colvanic ash chemistry on the soils and vegetation of naturally regenerated woodlands in the Massif Central, France. Catena 56, 239–261.
Rahman, S., Takaki, H., Tamai, M., Nagamoto, Y., 1996. Distribution of zinc, manganese, copper, cobalt and nickel in andosol profiles. Soil Science and Plant Nutrition 42 (4), 881–891.
Rockstrom, J., Barron, J., Fox, P., 2003. Water productivity in rainfed agriculture: Challenges and opportunities for smallholder farmers in drought-prone tropical agroecosystems. In: Kijne, J.W., Barker, R.A., Molden, D. (Eds.), Water Productivity in Agriculture: Limits and Opportunities for Improvement. CABI Publ., Oxon, Mass, pp. 145–162.
Røhr, P.C., Killingtveit, A., 2003. Rainfall distribution on the slopes of Mt. Kilimanjaro. Journal des Sciences Hydrologiques 48, 65–78.
Sak, P.B., Fisher, D.M., Gardner, T.W., Murphy, K., Brantley, S.L., 2003. Rates of weathering rind formation on Costa Rican basalt. Geochimica et Cosmochimica Acta 68 (7), 1453–1472.
Sastri, G.G.K., Sastry, C.S., 1982. Chemical characteristics and evolution of the laterite profile in Hazaridadar bauxite Plateau, Madhya Predesh, India. Economic Geology 77, 154–161.
Stocking, M.A., 2003. Tropical soils and food security—the next 50 years. Science 302, 1356–1359.
Sulkowski, M., Hirner, A.V., 2006. Element fractionation by sequential extraction in a soil with high carbonate content. Applied Geochemistry 21, 16–28.
Taylor, A., Blum, J.D., 1995. Relation between soil age and silicate weathering rates determined from the chemical evolution of a glacial chronosequence. Geology 23, 979–982.
Tessier, A., Campbell, P.G.C., Bisson, M., 1979. Sequential extraction prodecure for the speciation of particulate trace metals. Analytical Chemistry 51, 844–851.

Teutsch, N., Erel, Y., Halicz, L., Chadwick, O.A., 1999. The influence of rainfall on metal concentration and behavior in the soil. Geochimica et Cosmochimica Acta 63 (21), 3499–3511.

Vaje, P.I., Singh, B.R., Lal, R., 2005. Soil erosion and nutrient losses from a volcanic ash soil in Kilimanjaro Region, Tanzania. Journal of Sustainable Agriculture 26 (4), 95–117.

Velde, B., 1992. Introduction to Clay Minerals. Chapman & Hall, London.

Wilkinson, P., Mitchell, J.G., Cattermole, P.J., Downie, C., 1986. Volcanic chronology of the Meru-Kilimanjaro region, northern Tanzania. Journal of the Geological Society of London 143, 601–605.